Journal of Biomechanics 41 (2008) 2874–2883

Contents lists available at ScienceDirect

Journal of Biomechanics

journal homepage: www.elsevier.com/locate/jbiomech
www.JBiomech.com

Kinetic chain of overarm throwing in terms of joint rotations revealed by induced acceleration analysis

Masaya Hirashima [a,b,*], Katsu Yamane [c], Yoshihiko Nakamura [c], Tatsuyuki Ohtsuki [d]

[a] Department of Physical and Health Education, Graduate School of Education, University of Tokyo, 7-3-1 Hongo, Bunkyo-ku, Tokyo 113-0033, Japan
[b] Japan Society for the Promotion of Science, Chiyoda-ku, Tokyo 102-8472, Japan
[c] Department of Mechano-Informatics, Graduate School of Information Science and Technology, University of Tokyo, Bunkyo-ku, Tokyo 113-8656, Japan
[d] Department of Life Sciences, Graduate School of Arts and Sciences, University of Tokyo, Meguro-ku, Tokyo 153-8902, Japan

ARTICLE INFO

Article history:
Accepted 11 June 2008

Keywords:
Kinetic chain
Overarm throwing
Joint torque
Velocity-dependent torque
Induced acceleration analysis

ABSTRACT

This study investigated how baseball players generate large angular velocity at each joint by coordinating the joint torque and velocity-dependent torque during overarm throwing. Using a four-segment model (i.e., trunk, upper arm, forearm, and hand) that has 13 degrees of freedom, we conducted the induced acceleration analysis to determine the accelerations induced by these torques by multiplying the inverse of the system inertia matrix to the torque vectors. We found that the proximal joint motions (i.e., trunk forward motion, trunk leftward rotation, and shoulder internal rotation) were mainly accelerated by the joint torques at their own joints, whereas the distal joint motions (i.e., elbow extension and wrist flexion) were mainly accelerated by the velocity-dependent torques. We further examined which segment motion is the source of the velocity-dependent torque acting on the elbow and wrist accelerations. The results showed that the angular velocities of the trunk and upper arm produced the velocity-dependent torque for initial elbow extension acceleration. As a result, the elbow joint angular velocity increased, and concurrently, the forearm angular velocity relative to the ground also increased. The forearm angular velocity subsequently accelerated the elbow extension and wrist flexion. It also accelerated the shoulder internal rotation during the short period around the ball-release time. These results indicate that baseball players accelerate the distal elbow and wrist joint rotations by utilizing the velocity-dependent torque that is originally produced by the proximal trunk and shoulder joint torques in the early phase.

1. Introduction

Many coaches and scientists have explored the mechanism of overarm throws such as baseball pitching. Throws in baseball have been characterized in terms of muscle activity (Glousman et al., 1988; Hirashima et al., 2002), joint torque (Fleisig et al., 1995), and joint kinematics (Barrentine et al., 1998; Sakurai et al., 1993). However, knowledge of the cause-and-effect relation among these variables is severely lacking, although it is fundamental knowledge for improving and maintaining athletes' performance.

Understanding the cause-and-effect relation between the kinetics (e.g., muscle force, joint torque) and kinematics (e.g., joint rotation) is difficult in multi-joint movements, because the muscle torque at one joint induces angular accelerations at all the joints in the system due to the dynamic coupling (Zajac and Gordon, 1989). To deal with this issue, recent studies have introduced the forward dynamics approach (Zajac et al., 2002). They wrote the equations of motion of the multi-joint system in the following form:

$$\boldsymbol{I}(\boldsymbol{\theta})\ddot{\boldsymbol{\theta}} = \sum_{i=1}^{m} \boldsymbol{\tau}_i + \boldsymbol{V}(\boldsymbol{\theta}, \dot{\boldsymbol{\theta}}) + \boldsymbol{g}(\boldsymbol{\theta}) \quad (1)$$

where $\boldsymbol{\tau}_i$ is the torque vector produced by i-th muscle force. The accelerations induced by a muscle force can be calculated by multiplying the inverse of the system inertia matrix to the torque vector produced by the muscle force (i.e., $\boldsymbol{I}(\boldsymbol{\theta})^{-1}\boldsymbol{\tau}_i$). This forward dynamics analysis, which is often called *induced acceleration analysis,* can inform us about the degree of contribution of individual muscle forces for accelerating all the joints in the system. The induced acceleration analysis has been used in gait analysis to examine how individual muscle forces contribute to the forward and vertical acceleration of the body during walking (Anderson and Pandy, 2003; Kepple et al., 1997).

It should be noted that, as Eq. (1) indicates, angular accelerations are produced not only by the muscle and gravity torques, but also by the velocity-dependent torque. When the

* Corresponding author at: Department of Physical and Health Education, Graduate School of Education, University of Tokyo, 7-3-1 Hongo, Bunkyo-ku, Tokyo 113-0033, Japan. Tel./fax: +81 3 5841 3979.
E-mail address: hira@p.u-tokyo.ac.jp (M. Hirashima).

0021-9290/$ - see front matter © 2008 Elsevier Ltd. All rights reserved.
doi:10.1016/j.jbiomech.2008.06.014

Nomenclature

Notation for entire system

$\boldsymbol{\theta} \in \boldsymbol{R}^{13}$ generalized coordinates vector
$\dot{\boldsymbol{\theta}} \in \boldsymbol{R}^{13}$ generalized velocities vector
$\ddot{\boldsymbol{\theta}} \in \boldsymbol{R}^{13}$ generalized accelerations vector
$\boldsymbol{I}(\boldsymbol{\theta}) \in \boldsymbol{R}^{13 \times 13}$ system inertia matrix
$\boldsymbol{\tau} \in \boldsymbol{R}^{13}$ generalized forces vector (i.e., 3 forces and 10 torques)
$\boldsymbol{V}(\boldsymbol{\theta}, \dot{\boldsymbol{\theta}}) \in \boldsymbol{R}^{13}$ velocity-dependent torques vector
$\boldsymbol{g}(\boldsymbol{\theta}) \in \boldsymbol{R}^{13}$ gravity torques vector

Notation for each segment or joint: The number of subscript is used in such a manner that a segment and its proximal joint have the same number (i = 0: trunk, 1: upper arm or shoulder, 2: forearm or elbow, 3: hand or wrist)

$\boldsymbol{\omega}_i \in \boldsymbol{R}^3$ angular velocity vector of the *i*-th segment relative to the global coordinate system
$\boldsymbol{\Omega}_i \in \boldsymbol{R}^3$ angular velocity vector of the *i*-th joint coordinate system relative to the global coordinate system
$\dot{\boldsymbol{\theta}}_i \in \boldsymbol{R}^3$ *i*-th joint angular velocity vector
$\boldsymbol{L}_i \in \boldsymbol{R}^3$ vector pointing from the proximal joint to distal joint of *i*-th segment
$\boldsymbol{L}_{gi} \in \boldsymbol{R}^3$ vector pointing from the proximal joint to the center of mass of *i*-th segment

velocity-dependent torque is prominent during a sports movement such as baseball pitching, it is more difficult to determine the contribution of a muscle force to the system behavior. The muscle force at a certain instant not only produces *instantaneous* accelerations on the system, but also influences accelerations of the subsequent system through the velocity-dependent torque because the instantaneous accelerations accumulate in the system as the *velocity* (Fig. 1). Therefore, the muscle-induced accelerations calculated by the above method ($\boldsymbol{I}(\boldsymbol{\theta})^{-1}\boldsymbol{\tau}_i$) includes only the *instantaneous effects* from the muscle force at that instant. In contrast, the accelerations induced by the velocity-dependent torque ($\boldsymbol{I}(\boldsymbol{\theta})^{-1}\boldsymbol{V}(\boldsymbol{\theta}, \dot{\boldsymbol{\theta}})$) reflects the *cumulative effects* from all history of all muscles and gravity torques until that instant.

The capability of the algorithm to calculate these effects separately is suitable for the analysis of baseball pitching. In baseball pitching, the fastest possible speed at the hand is required, and eventually large angular accelerations are required. Because the instantaneous accelerations induced by the muscle force are limited by the muscle force-producing capacity, additional utilization of the velocity-dependent torque is very effective for producing larger angular accelerations than the muscle torque can produce on its own. Therefore, it is hypothesized that the control strategy of utilizing the velocity-dependent torque is adopted by baseball players. To test this hypothesis, it is necessary to examine the instantaneous and cumulative effects separately.

The effect of the velocity-dependent torque on the joint angular acceleration is related to the phenomena called "whip-like effect," "proximal-to-distal sequence," and "kinetic chain" (Atwater, 1979; Fleisig et al., 1996; Hore et al., 2005; Kibler, 1995; Marshall and Elliott, 2000). Although several researchers have tried to reveal its kinetic mechanism by using the equations of motion (Feltner, 1989; Feltner and Dapena, 1989; Hirashima et al., 2003, 2007b; Hong et al., 2001; Putnam, 1991, 1993), no study has accurately assessed the effect of the velocity-dependent torque on the joint angular accelerations. These studies dealt with the equation of each segment separately, and considered that each joint angular acceleration can be explained by the joint torque, gravity torque, and interaction (motion-dependent) torque. The critical problem is that the interaction torque includes angular accelerations of the other joints. This indicates that the previous studies explained the cause of an angular acceleration by using the other angular accelerations, although, actually, all of the angular accelerations in a multi-joint system must be determined simultaneously (for detailed discussion see Hirashima and Ohtsuki, in press).

The first purpose of this paper was to apply the induced acceleration analysis to baseball pitching and examine how the velocity-dependent torque contributes to each joint angular acceleration. Second, we examined which segment motion is the source of the velocity-dependent torque by decomposing the velocity-dependent torque into some kinematic sources.

2. Methods

2.1. Movements and recording

We analyzed the pitching motions of six right-handed baseball players. Five were varsity baseball players (mean age: 19.8 yr) and one had been a professional baseball player (42 yr). After submitting written informed consent, each participant threw straight balls with the right-hand aiming at a target under three different speed conditions: slow accurate, medium accurate, and fast accurate. In this paper, we analyzed three fast throws for each participant (ball speed: 28.1 ± 1.92 m/s). Eleven spherical reflective markers (1.5 cm in diameter) were used to identify anatomical landmarks. Marker position data were recorded at 200 Hz. The 3D reconstruction error was 2.65 mm in average. The data were smoothed by applying the bidirectional fourth-order Butterworth low-pass filter. The cutoff frequency was calculated for each marker by residual analysis (Winter, 1990). The average cutoff frequency was 14.1 Hz for the trunk and shoulder markers and 20.1 Hz for the more distal markers. To reduce the error of numerical differentiation, the data were resampled at 2000 Hz by the spline interpolation. Data came from a previous study (Hirashima et al., 2007b), and a detailed procedure was described there.

2.2. Inverse kinematics

We used a four-segment model (trunk, upper arm, forearm, and hand plus ball[1]) that has 13 DOFs[2] (Fig. 2). In order to obtain kinematic data which are valid for the link segment model, we used the *inverse kinematics* technique (Lu and O'Connor, 1999; Yamane and Nakamura, 2003b). This method calculates all the joint angles simultaneously so that the virtual markers fixed on the model (green markers in Fig. 3) maximally fit each corresponding motion-captured markers (magenta markers). The time-averaged values of distance between the motion-captured markers and virtual markers on the model are <4 mm for the wrist and MP markers, and <7 mm for other proximal markers on average (Table 1).

2.3. Inverse dynamics

The equations of motion for the four-segment model can be derived in a similar manner as in a previous paper (Hirashima et al., 2007a):

$$\boldsymbol{I}(\boldsymbol{\theta})\ddot{\boldsymbol{\theta}} = \boldsymbol{\tau} + \boldsymbol{V}(\boldsymbol{\theta}, \dot{\boldsymbol{\theta}}) + \boldsymbol{g}(\boldsymbol{\theta}) \quad (2)$$

We calculated the generalized forces by substituting the model-valid kinematics and subject's segment parameters (Ae et al., 1992) into Eq. (3),

$$\boldsymbol{\tau} = \boldsymbol{I}(\boldsymbol{\theta})\ddot{\boldsymbol{\theta}} - \boldsymbol{V}(\boldsymbol{\theta}, \dot{\boldsymbol{\theta}}) - \boldsymbol{g}(\boldsymbol{\theta}) \quad (3)$$

[1] The ball was removed after the time of ball release.

[2] The model has 13 DOFs (6 for trunk, 3 for shoulder, 2 for elbow, and 2 for wrist). The complete definition of each joint coordinate axis is described in the Appendix.

2.4. Induced acceleration analysis

Angular accelerations produced by torques were calculated by the following equation:

$$\ddot{\boldsymbol{\theta}} = \boldsymbol{I}(\boldsymbol{\theta})^{-1}(\boldsymbol{\tau} + \boldsymbol{V}(\boldsymbol{\theta}, \dot{\boldsymbol{\theta}}) + \boldsymbol{g}(\boldsymbol{\theta})) \tag{4}$$

This equation tells us that the j-th angular acceleration ($\ddot{\theta}_j$) is produced by the 13 generalized forces, velocity-dependent torques, and gravity torques as follows:

$$\begin{aligned}\ddot{\theta}_j &= \sum_{i=1}^{13} A_{ji}\tau_i + \sum_{i=1}^{13} A_{ji}V_i + \sum_{i=1}^{13} A_{ji}g_i \\ &= (\ddot{\theta}_j^{\tau 1} + \ddot{\theta}_j^{\tau 2} + \cdots + \ddot{\theta}_j^{\tau 13}) + \ddot{\theta}_j^{V} + \ddot{\theta}_j^{g}\end{aligned} \tag{5}$$

where A_{ji} is the (j, i) component of the matrix $\boldsymbol{I}(\boldsymbol{\theta})^{-1}$. To confirm whether the accelerations calculated by Eq. (4) reproduce the original kinematics, we conducted the forward dynamics simulation. It reproduced the original kinematics with good tolerance (Table 2).

2.5. Decomposition of the velocity-dependent torque

By carefully inspecting the mathematical terms of the velocity-dependent torque, we found that it can be expressed as the sum of several kinematic variables as follows:

$$\boldsymbol{V}(\boldsymbol{\theta}, \dot{\boldsymbol{\theta}}) = \sum_{i=0}^{3}\{\boldsymbol{V}_{A_i}(\boldsymbol{A}_i) + \boldsymbol{V}_{B_i}(\boldsymbol{B}_i) + \boldsymbol{V}_{B_{gi}}(\boldsymbol{B}_{gi}) + \boldsymbol{V}_{C_i}(\boldsymbol{C}_i)\} \tag{6}$$

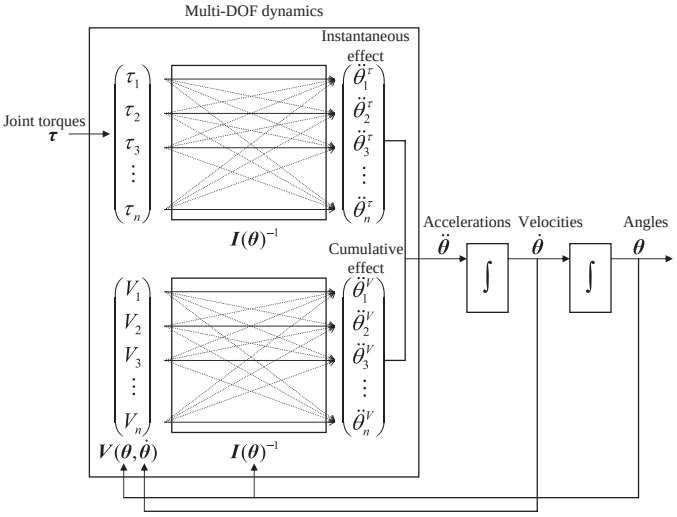

Fig. 1. Block diagram of the generation mechanism of multi-DOF human motion. The upper part indicates the instantaneous effect produced by the joint torque. The lower part indicates the cumulative effect produced by the velocity-dependent torque. The gravity torque is not shown here. The solid line indicates the direct effect from its own torque. The dotted line indicates the remote effect from the other torques.

where the subscript i indicates the segment number and

$$\begin{aligned}\boldsymbol{A}_i &= \boldsymbol{\Omega}_i \times (\dot{\boldsymbol{\theta}}_i) \\ \boldsymbol{B}_i &= \boldsymbol{\omega}_i \times (\boldsymbol{\omega}_i \times \boldsymbol{L}_i) \\ \boldsymbol{B}_{gi} &= \boldsymbol{\omega}_i \times (\boldsymbol{\omega}_i \times \boldsymbol{L}_{gi}) \\ \boldsymbol{C}_i &= \boldsymbol{\omega}_i \times (\boldsymbol{I}_i\boldsymbol{\omega}_i)\end{aligned} \tag{7}$$

The velocity-dependent torque was decomposed into 15 components (i.e., $4 \times 4 - 1$), because $\boldsymbol{B}_3$ does not appear.

2.6. Integration of angular acceleration

To evaluate the contribution of each torque to the large angular velocities at ball release, we calculated the integral of the acceleration produced by each torque from −200 to 0 ms for the shoulder, elbow, and wrist. For the trunk, we integrated the accelerations from −200 ms to the time of peak velocity to examine the contribution of each torque to the peak velocity rather than the velocity at ball release. This is because the point of this study is to understand the cause of the large angular velocity of the trunk in the early phase that would be the cause of the velocity-dependent torque at the distal joints in the later phase.

3. Results

3.1. Induced acceleration analysis

3.1.1. Trunk

The forward translational motion of the trunk (Fig. 4a) started earlier than the leftward rotation (Fig. 5a). The initial forward

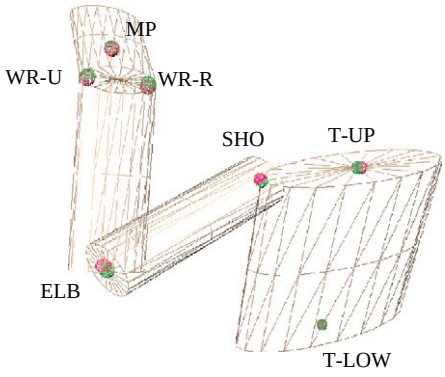

Fig. 3. Seven markers that were used in the inverse kinematics. The inverse kinematics calculates all joint angles simultaneously so that the virtual markers fixed on the segments (green markers) maximally fit each corresponding motion-captured markers (magenta markers). The radius of spheres in this graphics is 10 mm. T-LOW, lower marker of the trunk; T-UP, upper marker of the trunk; SHO, shoulder joint center; ELB, elbow joint center; WR-R, radial side of the wrist; WR-U, ulnar side of the wrist; MP, metacarpophalangeal joint of the middle finger. (For the interpretation of color please see the figure in the web version).

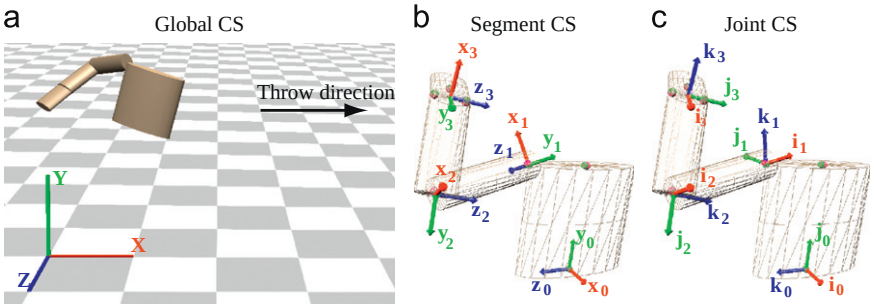

Fig. 2. (a) The global coordinate system (CS). (b) Segment-fixed coordinate systems for the trunk, upper arm, forearm, and hand. (c) Joint coordinate systems for the trunk, shoulder, elbow, and wrist.

Table 1
Time-averaged values of the distance (mm) between motion-captured markers and virtual markers on the model for all subjects

	T-LOW	T-UP	SHO	ELB	WR-U	WR-R	MP
Subject A	0.62	3.85	4.37	4.21	2.68	2.09	3.66
Subject B	1.32	7.79	7.49	7.62	3.42	3.38	2.68
Subject C	0.78	5.30	4.12	6.27	3.11	2.65	2.84
Subject D	2.14	9.23	6.36	7.95	4.02	3.11	3.94
Subject E	0.71	5.65	4.65	5.02	2.25	2.11	3.69
Subject F	1.07	6.00	4.35	6.07	3.22	2.97	2.46
Average	1.11	6.30	5.22	6.19	3.12	2.72	3.21

Table 2
Distance (mm) between the markers of the model-valid kinematics and those of the simulated motion at the ball-release time (0 ms)

	T-LOW	T-UP	SHO	ELB	WR-U	WR-R	MP
Subject A	2.14	0.73	0.74	0.76	2.69	4.19	1.61
Subject B	3.43	1.39	1.14	1.25	7.09	6.45	3.84
Subject C	0.78	0.53	1.19	1.91	1.78	4.10	2.75
Subject D	5.71	4.26	2.68	4.25	8.44	7.34	10.53
Subject E	1.51	0.28	0.55	1.51	7.61	9.30	2.33
Subject F	0.86	0.91	1.81	2.59	1.30	3.56	3.00
Average	2.41	1.35	1.35	2.05	4.82	5.82	4.01

Numerical integration was conducted from −150 to 0 ms by the Runge–Kutta algorithm with a constant time step of 0.25 ms.

acceleration (solid black during gray area in Fig. 4b) was mainly induced by the forward force at the trunk (solid cyan). The leftward angular acceleration (solid black during gray area in Fig. 5b) was mainly produced by the leftward rotation torque at the trunk (dotted magenta) with the counteraction by the shoulder horizontal flexion torque (dash red). The velocity-dependent torque (dotted black) had little contribution to the accelerations of both translational and angular motions.

3.1.2. Shoulder

Although the shoulder rotated externally up to about −30 ms, the angular velocity of the internal rotation rapidly increased as the time of ball release approached (Fig. 6a). The angular velocity often reached its peak just after the ball release. The angular acceleration was mainly produced by the internal rotation torque at the shoulder (solid red in Fig. 6b). Although the velocity-dependent torque (dotted black) decelerated the internal rotation up to −10 ms, it accelerated the internal rotation during the very short period around the ball-release time.

The angular velocity and acceleration of the shoulder horizontal flexion were kept low (Figs. 7a and b) in comparison with those of the shoulder internal rotation, because the horizontal flexion torque at the shoulder (dash red in Figs. 7b) and the leftward torque at the trunk (dotted magenta) counteracted each other.

3.1.3. Elbow

The elbow was initially flexed (∼−130 ms), and then extended as the time of ball release approached (Fig. 8a). The extension angular velocity often reached its peak just before ball release. The elbow extension acceleration was mainly produced by the velocity-dependent torque (dotted black line in Fig. 8b). Although the elbow joint torque initially accelerated the elbow extension in some subjects (solid green around −100 to −50 ms), it strongly decelerated the elbow extension during 20 ms before the ball release in all subjects.

3.1.4. Wrist

The wrist was initially extended (∼−50 ms), and then flexed as the time of ball release approached (Fig. 9a). The wrist flexion acceleration was produced by the velocity-dependent torque (dotted black line in Fig. 9b), horizontal flexion torque at the shoulder (dash red), elbow flexion torque (solid green), and wrist flexion torque (dotted blue, −100 to −20 ms) with a strong counteraction by the internal rotation torque at the shoulder (solid red) and wrist extension torque (dotted blue, −20 to +10 ms).

3.1.5. Across-subject data

The across-subjects averages of the integrals of the accelerations indicated that above observations were consistent across subjects. The proximal trunk and shoulder joint motions were mainly accelerated by the joint forces and torques at their own joints (Figs. 4d, 5d, 6d, and 7d), whereas the distal elbow and wrist motions were mainly accelerated by the velocity-dependent torque (Figs. 8d and 9d).

3.2. Decomposition of velocity-dependent torque

Fig. 10a shows the internal rotation accelerations at the shoulder produced by the 15 components in the velocity-dependent torque (Eqs. (6) and (7)). The forearm angular velocity-dependent torques (A_2, dotted green; B_2, solid green) contributed to the deceleration up to −10 ms. The forearm angular velocity-dependent torques (A_2, dotted green; B_2, solid green; B_{g2}, dash green; C_2, chain green) contributed to the acceleration during the very short period around the ball-release time.

Data for the elbow extension (Fig. 10c) indicated that initial acceleration (∼−50 ms) produced by the velocity-dependent torque were mainly contributed by the trunk angular velocity-dependent torque (B_0, solid magenta) and upper arm angular velocity-dependent torque (B_1, solid red). Later (from −50 to 0 ms), the forearm angular velocity-dependent torque (B_{g2}, dash green) became the main contributor.

Data for the wrist flexion (Fig. 10e) indicated that the acceleration produced by the velocity-dependent torque were mainly contributed by the forearm angular velocity-dependent torques (B_2, solid green). These observations were consistent across subjects (Figs. 10b, d, and f).

4. Discussion

Although the proximal-to-distal sequence during overarm throws has been long reported (Atwater, 1979), the kinetic mechanism that causes this sequence remains unclear. To assess this mechanism, the present study examined how the joint torque and velocity-dependent torque contribute to each joint angular acceleration during baseball pitching, using the induced acceleration analysis. In the early phase from −200 to −100 ms, the trunk motion was produced by the trunk force and torque (Figs. 4b and 5b). The shoulder horizontal flexion torque during this phase prevented the upper arm from lagging behind relative to the trunk (Fig. 7b). Thus, the angular velocity of the upper arm also increased with that of the trunk. This result is consistent with the basic assumption of the kinetic chain that the proximal segment motions are generated by the powerful muscles located in the proximal segments (Fleisig et al., 1996; Kibler, 1995). In contrast, the distal elbow and wrist joint rotations were mainly accelerated by the velocity-dependent torque rather than the joint torque (Figs. 8b and 9b). Although this concept has been also suggested by the interaction torque analysis (Feltner, 1989;

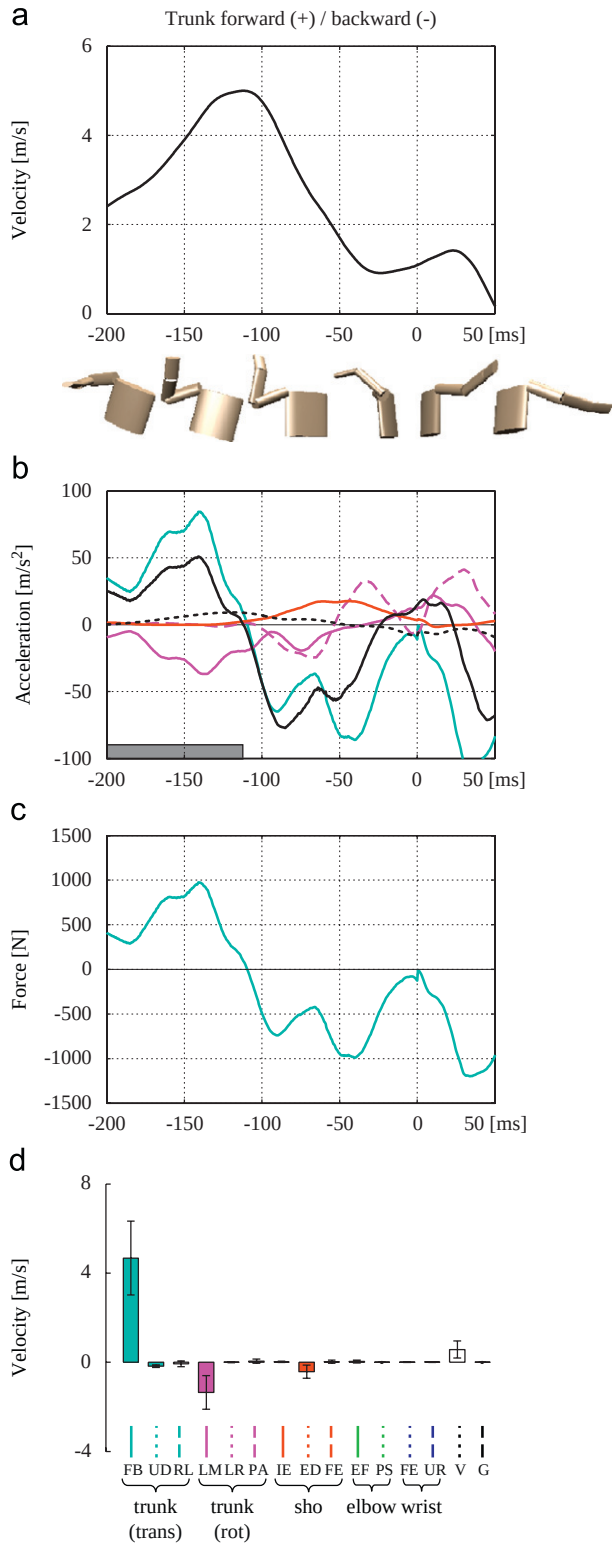

Fig. 4. Data describing the trunk forward/backward translational motion of a representative single trial: (a) velocity, (b) acceleration (solid black) and its 15 components. Only major contributors are shown, (c) force, (d) integrated value of the 15 accelerations during the interval indicated by the gray bar in (b). FB, forward/backward (solid cyan); UD, upward/downward (dotted cyan); RL, Right/left (dash cyan) of the trunk translational motion; LM, lateral/medial (solid magenta); LR, leftward/rightward (dotted magenta); PA, posterior/anterior (dash magenta) of the trunk rotation; IE, internal/external rotation (solid red); ED, elevation/depression (dotted red); FE, horizontal flexion/extension (dash red) at the shoulder; EF, extension/flexion (solid green); PS, pronation/supination (dotted green) at the elbow; FE, flexion/extension (dotted blue); UR, ulnar/radial deviation (dash blue) at the wrist; V, velocity-dependent torque (dotted black); G, gravity torque (dash black). (For the interpretation of color please see the figure in the web version).

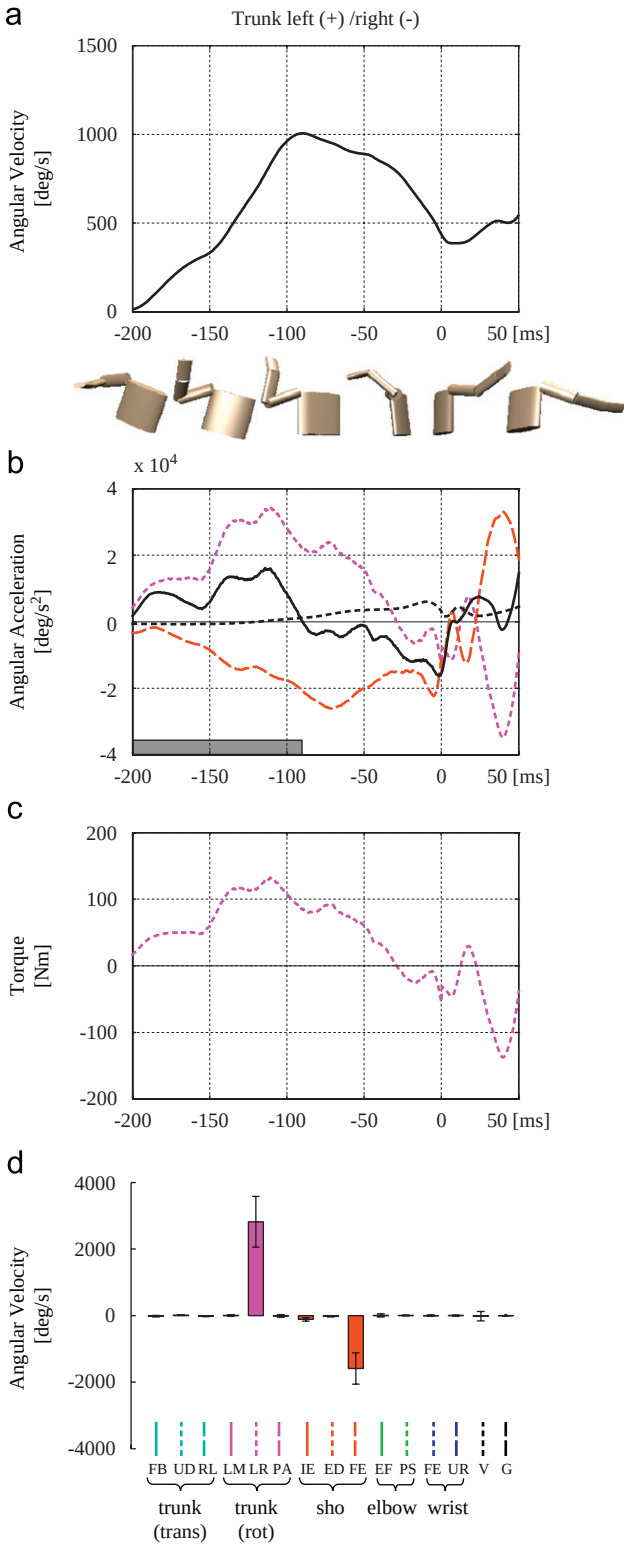

Fig. 5. Data describing the trunk leftward/rightward rotation of the representative single trial (same as Fig. 4): (a) angular velocity, (b) angular acceleration (solid black) and its 15 components. Only major contributors are shown, (c) torque, (d) integrated value of the 15 accelerations during the interval indicated by the gray bar in (b). FB, forward/backward (solid cyan); UD, upward/downward (dotted cyan); RL, right/left (dash cyan) of the trunk translational motion; LM, lateral/medial (solid magenta); LR, leftward/rightward (dotted magenta); PA, posterior/anterior (dash magenta) of the trunk rotation; IE, internal/external rotation (solid red); ED, elevation/depression (dotted red); FE, horizontal flexion/extension (dash red) at the shoulder; EF, extension/flexion (solid green); PS, pronation/supination (dotted green) at the elbow; FE, flexion/extension (dotted blue); UR, ulnar/radial deviation (dash blue) at the wrist; V, velocity-dependent torque (dotted black); G, gravity torque (dash black). (For the interpretation of color please see the figure in the web version).

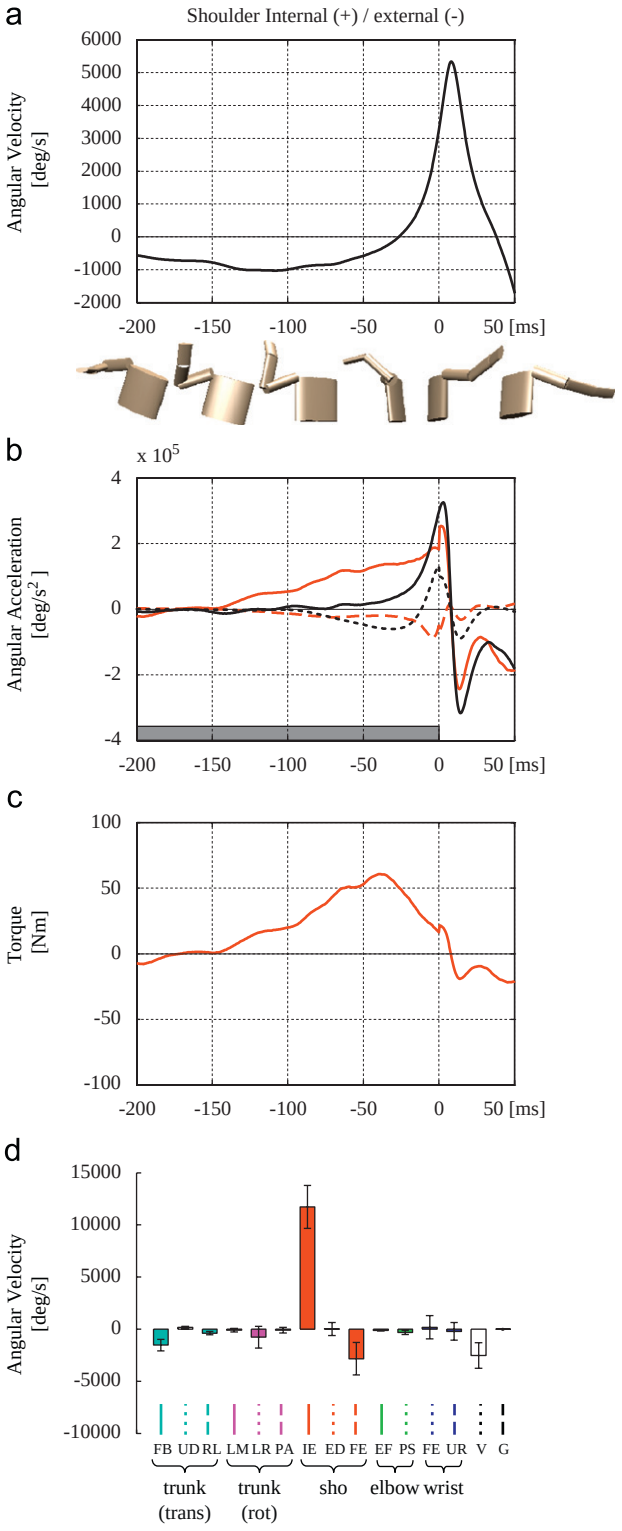

Fig. 6. Data describing the shoulder internal/external rotation of the representative single trial (same as Fig. 4): (a) angular velocity, (b) angular acceleration (solid black) and its 15 components. Only major contributors are shown: (c) torque, (d) integrated value of the 15 accelerations during the interval indicated by the gray bar in (b). FB, forward/backward (solid cyan); UD, upward/downward (dotted cyan); RL, right/left (dash cyan) of the trunk translational motion; LM, lateral/medial (solid magenta); LR, leftward/rightward (dotted magenta); PA, posterior/anterior (dash magenta) of the trunk rotation; IE, internal/external rotation (solid red); ED, elevation/depression (dotted red); FE, horizontal flexion/extension (dash red) at the shoulder; EF, extension/flexion (solid green); PS, pronation/supination (dotted green) at the elbow; FE, flexion/extension (dotted blue); UR, ulnar/radial deviation (dash blue) at the wrist; V, velocity-dependent torque (dotted black); G, gravity torque (dash black). (For the interpretation of color please see the figure in the web version).

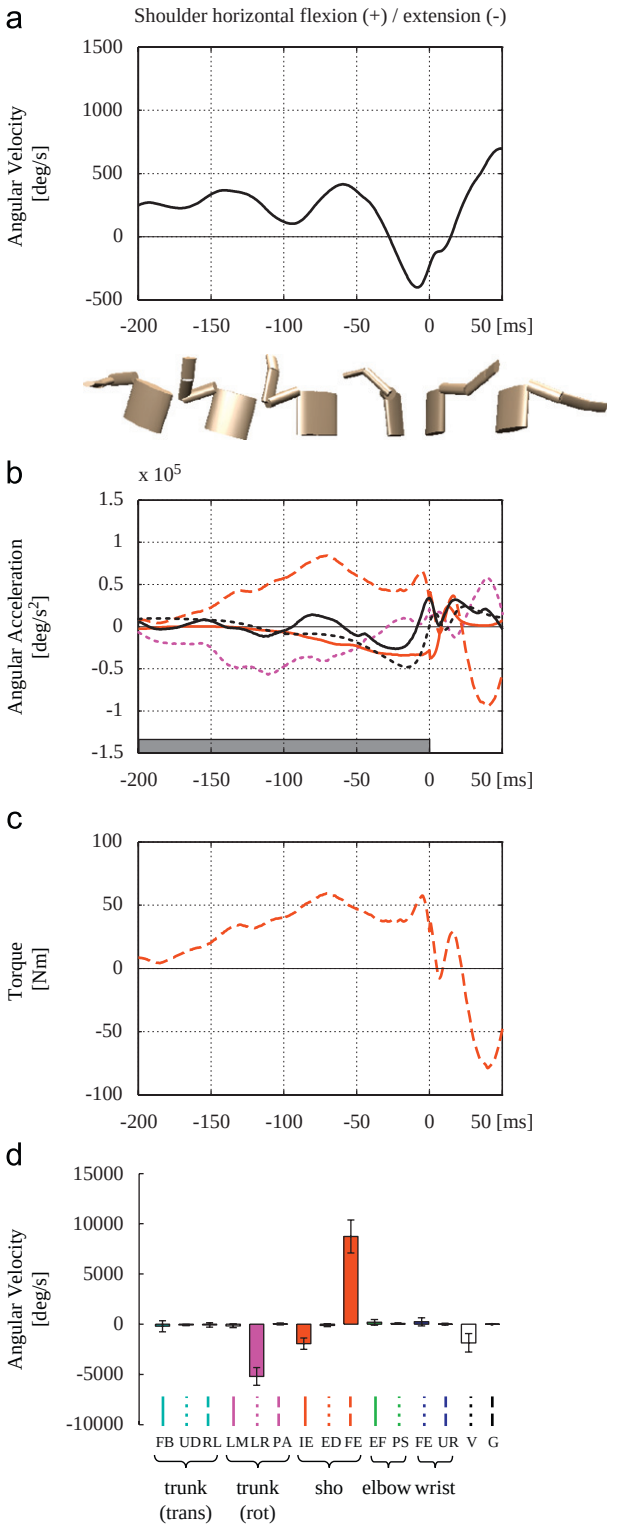

Fig. 7. Data describing the shoulder horizontal flexion/extension of the representative single trial (same as Fig. 4): (a) angular velocity, (b) angular acceleration (solid black) and its 15 components. Only major contributors are shown: (c) torque, (d) integrated value of the 15 accelerations during the interval indicated by the gray bar in (b). FB, forward/backward (solid cyan); UD, upward/downward (dotted cyan); RL, right/left (dash cyan) of the trunk translational motion; LM, lateral/medial (solid magenta); LR, leftward/rightward (dotted magenta); PA, posterior/anterior (dash magenta) of the trunk rotation; IE, internal/external rotation (solid red); ED, elevation/depression (dotted red); FE, horizontal flexion/extension (dash red) at the shoulder; EF, extension/flexion (solid green); PS, pronation/supination (dotted green) at the elbow; FE, flexion/extension (dotted blue); UR, ulnar/radial deviation (dash blue) at the wrist; V, velocity-dependent torque (dotted black); G, gravity torque (dash black). (For the interpretation of color please see the figure in the web version).

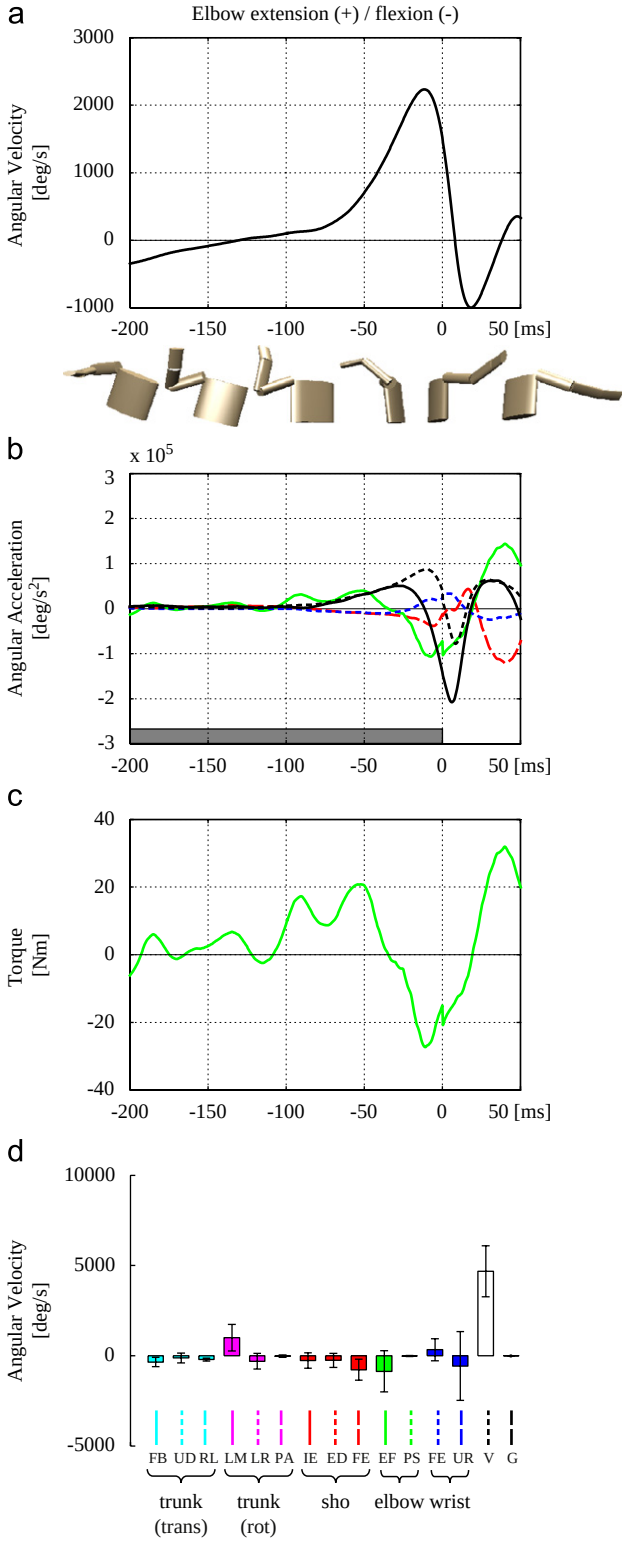

Fig. 8. Data describing the elbow extension/flexion of the representative single trial (same as Fig. 4): (a) angular velocity, (b) angular acceleration (solid black) and its 15 components. Only major contributors are shown: (c) torque, (d) integrated value of the 15 accelerations during the interval indicated by the gray bar in (b). FB, forward/backward (solid cyan); UD, upward/downward (dotted cyan); RL, right/left (dash cyan) of the trunk translational motion; LM, lateral/medial (solid magenta); LR, leftward/rightward (dotted magenta); PA, posterior/anterior (dash magenta) of the trunk rotation; IE, internal/external rotation (solid red); ED, elevation/depression (dotted red); FE, horizontal flexion/extension (dash red) at the shoulder; EF, extension/flexion (solid green); PS, pronation/supination (dotted green) at the elbow; FE, flexion/extension (dotted blue); UR, ulnar/radial deviation (dash blue) at the wrist; V, velocity-dependent torque (dotted black); G, gravity torque (dash black). (For the interpretation of color please see the figure in the web version).

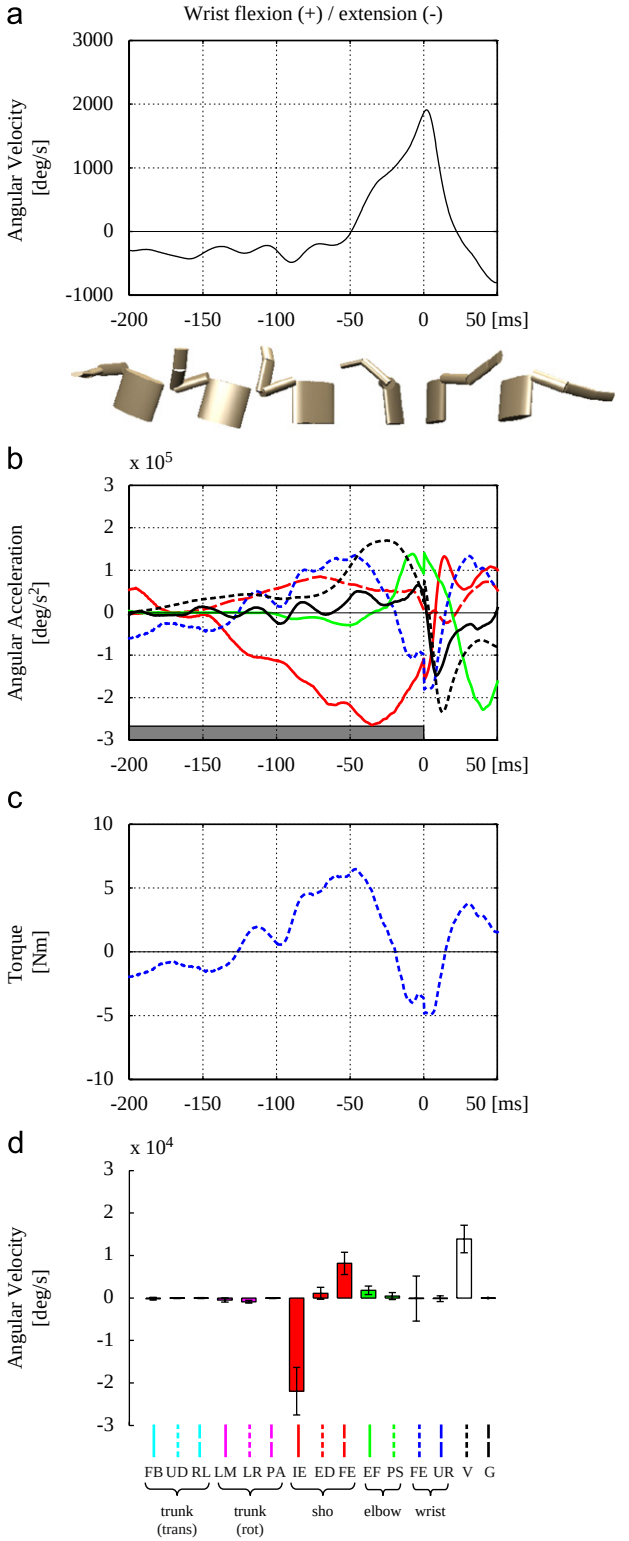

Fig. 9. Data describing the wrist flexion/extension of the representative single trial (same as Fig. 4): (a) angular velocity, (b) angular acceleration (solid black) and its 15 components. Only major contributors are shown: (c) torque, (d) integrated value of the 15 accelerations during the interval indicated by the gray bar in (b). FB, forward/backward (solid cyan); UD, upward/downward (dotted cyan); RL, right/left (dash cyan) of the trunk translational motion; LM, lateral/medial (solid magenta); LR, leftward/rightward (dotted magenta); PA, posterior/anterior (dash magenta) of the trunk rotation; IE, internal/external rotation (solid red); ED, elevation/depression (dotted red); FE, horizontal flexion/extension (dash red) at the shoulder; EF, extension/flexion (solid green); PS, pronation/supination (dotted green) at the elbow; FE, flexion/extension (dotted blue); UR, ulnar/radial deviation (dash blue) at the wrist; V, velocity-dependent torque (dotted black); G, gravity torque (dash black). (For the interpretation of color please see the figure in the web version).

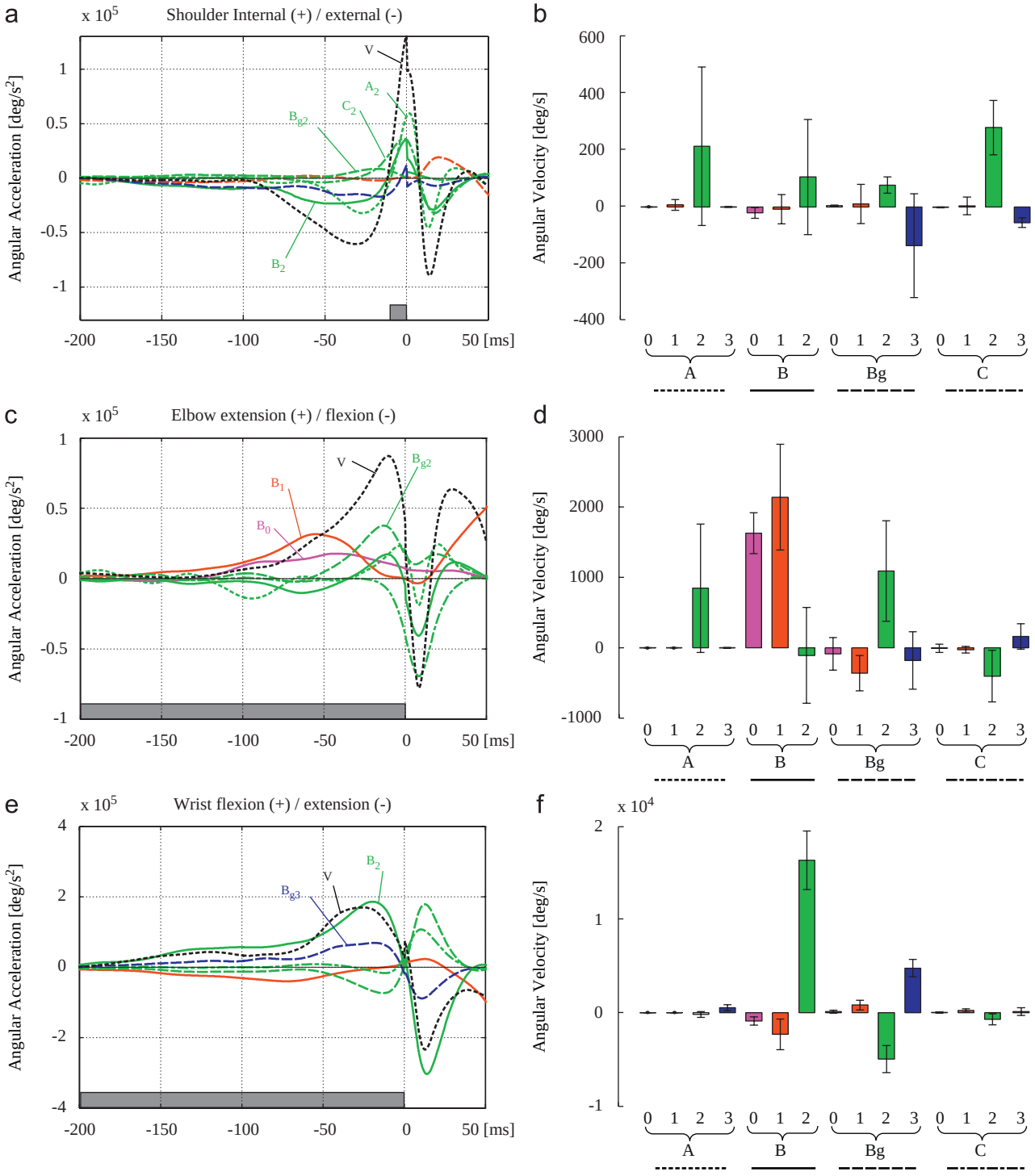

Fig. 10. Details of the acceleration induced by the velocity-dependent torque at the shoulder internal/external rotation (a), elbow extension/flexion (c), and wrist flexion/extension (e) of the representative single trial (same as Fig. 4). (b, d, f) Integrated values during the interval indicated by the gray bar in (a), (c), and (e), respectively. The characters in the legend (A, B, Bg, C) indicate the components shown in Eq. (7). The numbers in the legend (0, 1, 2, 3) indicate the segment number: 0, trunk (magenta); 1, upper arm (red); 2, forearm (green); 3, hand (blue). (For the interpretation of color please see the figure in the web version).

Hirashima et al., 2003, 2007b; Putnam, 1993), their methods have low reliability due to the incorrect interpretation of the cause-and-effect relation between torques and accelerations (see Introduction), and hence they can never accurately determine the original cause of the interaction torque. The strength of the present study is that we further traced the original cause of the velocity-dependent torque by decomposing the velocity-dependent torque into some kinematic sources. Results showed that the velocity-dependent torques at the shoulder, elbow, and wrist were produced by the forearm angular velocity that was originally produced by the trunk and shoulder joint torques in earlier phase.

It should be noted that the mechanism of the cumulative effect is different from the mechanism of the "torque reversal"

examined by Chowdhary and Challis (2001) and Herring and Chapman (1992). They demonstrated, using simulations, that the braking of a proximal segment accelerated the distal segment and was effective for generating the fastest throw. In the present study, the elbow joint torque reversed its direction from extension to flexion at about −40 ms (Fig. 8c). While the elbow flexion torque decelerated the elbow extension (solid green in Fig. 8b), it accelerated the distal wrist flexion (solid green in Fig. 9b). Thus, the positive effect of the torque reversal is one of the *instantaneous effects* from the *remote* joint torques (dotted line on the upper panel in Fig. 1). Therefore, this effect is not influenced by the proximal joint torques in the early phase in contrast to the cumulative effect. In spite of the clear difference between the instantaneous remote effect and cumulative effect, no study has clearly stated this difference on this point. This would be because the two effects are similar, in that they are caused by the torques other than the *direct* joint torque. In fact, both effects have been classified into the category of interaction torque (Hirashima et al., 2003, 2007b; Hollerbach and Flash, 1982; Putnam, 1993).

It is also important to note that the kinetic chain mechanism is determined not only by the magnitudes of the joint torques and angular velocities, but also by the *limb posture*, because the limb posture influences the system inertia matrix. This effect is clearly seen at the shoulder internal rotation. Fig. 6b shows that the acceleration induced by the shoulder internal rotation torque (solid red) reached its peak around the ball release, whereas the torque itself reached its peak at about −50 ms (Fig. 6c). As the time of ball release approached, the elbow extended near full extension, and concurrently, the value of the inertial matrix related to the shoulder internal rotation axis became small. Thus, the acceleration induced by the torque became large at ball release, even if the magnitude of the torque was relatively small. This increase of effectiveness of the joint torque would be one reason why baseball players extend the elbow before the shoulder internal rotation, which cannot be explained by the traditional proximal-to-distal principle (Marshall and Elliott, 2000). The velocity-dependent torque would be also related to the elbow-to-shoulder sequence. It might be that the forearm angular velocity-dependent torque can be utilized for the shoulder internal rotation just before the ball release (Fig. 10a), only if this sequence is used. In addition, the negative effect from the velocity-dependent torque from −100 to −10 ms (dotted black in Fig. 6b) played a role to form the elbow-to-shoulder sequence, because it contributed to delay the shoulder internal rotation. The negative effect is also related to the stretch-shortening cycle because it contributed to stretch the muscles and joint structures much more than without it. The large joint torque around −40 ms (Fig. 6c) would be generated by the passive elasticity of these elements (O'Brien et al., 1990).

In conclusion, the present study provided the clear picture of the kinetic chain during overarm throwing: the segmental sequence is produced by the utilization of the cumulative effect, instantaneous remote effect, and effective limb posture. Furthermore, we developed the method to determine the original cause of the cumulative effect, and revealed the route of the kinetic chain. This clear knowledge about the chain of causation is essential to provide useful advices for throwing athletes.

However, there is one limitation about the induced acceleration analysis. Chen (2006) raised one problem that the number of segment of the model affects the interpretation of the function of joint torques. Patel et al. (2007) also reported that the role of the hip joint torque during walking differed depending on the model used. To examine whether the present result about overarm throwing is robust or not, future studies need to examine the overarm throwing with a more accurate model that includes the non-throwing arm, finger joints, or the lower extremity with foot ground contacts (Yamane and Nakamura, 2003a).

Conflict of interest statement

None of the authors have any conflicts of interest associated with this study.

Acknowledgment

This research was supported by Grants-in-Aid for JSPS Fellows (No. 19-8779).

Appendix A. Supporting Information

Supplementary data associated with this article can be found in the online version at doi:10.1016/j.jbiomech.2008.06.014

References

Ae, M., Tang, H., Yokoi, T., 1992. Estimation of inertia properties of the body segments in Japanese athletes. In: Society of Biomechanisms (Ed.), Biomechanisms 11, vol.7. Tokyo Daigaku Shuppan-Kai, Tokyo, pp. 23–33.

Anderson, F.C., Pandy, M.G., 2003. Individual muscle contributions to support in normal walking. Gait and Posture 17, 159–169.

Atwater, A.E., 1979. Biomechanics of overarm throwing movements and of throwing injuries. Exercise and Sport Sciences Reviews 7, 43–85.

Barrentine, S.W., Matsuo, T., Escamilla, R.F., Fleisig, G.S., Andrews, J.R., 1998. Kinematic analysis of the wrist and forearm during baseball pitching. Journal of Applied Biomechanics 14, 24–39.

Chen, G., 2006. Induced acceleration contributions to locomotion dynamics are not physically well defined. Gait and Posture 23, 37–44.

Chowdhary, A.G., Challis, J.H., 2001. The biomechanics of an overarm throwing task: a simulation model examination of optimal timing of muscle activations. Journal of Theoretical Biology 211, 39–53.

Feltner, M.E., 1989. 3-dimensional interactions in a 2-segment kinetic chain. 2. Application to the throwing arm in baseball pitching. International Journal of Sport Biomechanics 5, 420–450.

Feltner, M.E., Dapena, J., 1989. 3-dimensional interactions in a 2-segment kinetic chain. 1. General-model. International Journal of Sport Biomechanics 5, 403–419.

Fleisig, G.S., Andrews, J.R., Dillman, C.J., Escamilla, R.F., 1995. Kinetics of baseball pitching with implications about injury mechanisms. American Journal of Sports Medicine 23, 233–239.

Fleisig, G.S., Barrentine, S.W., Escamilla, R.F., Andrews, J.R., 1996. Biomechanics of overhand throwing with implications for injuries. Sports Medicine 21, 421–437.

Glousman, R., Jobe, F., Tibone, J., Moynes, D., Antonelli, D., Perry, J., 1988. Dynamic electromyographic analysis of the throwing shoulder with glenohumeral instability. Journal of Bone and Joint Surgery—American Volume 70A, 220–226.

Herring, R.M., Chapman, A.E., 1992. Effects of changes in segmental values and timing of both torque and torque reversal in simulated throws. Journal of Biomechanics 25, 1173–1184.

Hirashima, M., Kadota, H., Sakurai, S., Kudo, K., Ohtsuki, T., 2002. Sequential muscle activity and its functional role in the upper extremity and trunk during overarm throwing. Journal of Sports Sciences 20, 301–310.

Hirashima, M., Kudo, K., Ohtsuki, T., 2003. Utilization and compensation of interaction torques during ball-throwing movements. Journal of Neurophysiology 89, 1784–1796.

Hirashima, M., Kudo, K., Ohtsuki, T., 2007a. A new non-orthogonal decomposition method to determine effective torques for three-dimensional joint rotation. Journal of Biomechanics 40, 871–882 (Erratum. Journal of Biomechanics 41, 488–489, 2008).

Hirashima, M., Kudo, K., Watarai, K., Ohtsuki, T., 2007b. Control of 3D limb dynamics in unconstrained overarm throws of different speeds performed by skilled baseball players. Journal of Neurophysiology 97, 680–691.

Hirashima, M., Ohtsuki, T., in press. Exploring the mechanism of skilled overarm throwing. Exercise and Sport Sciences Reviews.

Hollerbach, J.M., Flash, T., 1982. Dynamic interactions between limb segments during planar arm movement. Biological Cybernetics 44, 67–77.

Hong, D.A., Cheung, T.K., Roberts, E.M., 2001. A three-dimensional, six-segment chain analysis of forceful overarm throwing. Journal of Electromyography and Kinesiology 11, 95–112.

Hore, J., Debicki, D.B., Watts, S., 2005. Braking of elbow extension in fast overarm throws made by skilled and unskilled subjects. Experimental Brain Research 164, 365–375.

Kepple, T.M., Siegel, K.L., Stanhope, S.J., 1997. Relative contributions of the lower extremity joint moments to forward progression and support during gait. Gait and Posture 6, 1–8.

Kibler, W.B., 1995. Biomechanical analysis of the shoulder during tennis activities. Clinics in Sports Medicine 14, 79–85.

Lu, T.W., O'Connor, J.J., 1999. Bone position estimation from skin marker co-ordinates using global optimisation with joint constraints. Journal of Biomechanics 32, 129–134.

Marshall, R.N., Elliott, B.C., 2000. Long-axis rotation: the missing link in proximal-to-distal segmental sequencing. Journal of Sports Sciences 18, 247–254.

O'Brien, S.J., Neves, M.C., Arnoczky, S.P., Rozbruck, S.R., Dicarlo, E.F., Warren, R.F., Schwartz, R., Wickiewicz, T.L., 1990. The anatomy and histology of the inferior glenohumeral ligament complex of the shoulder. American Journal of Sports Medicine 18, 449–456.

Patel, M., Talaty, M., Ounpuu, S., 2007. The impact of adding trunk motion to the interpretation of the role of joint moments during normal walking. Journal of Biomechanics 40, 3563–3569.

Putnam, C.A., 1991. A segment interaction analysis of proximal-to-distal sequential segment motion patterns. Medicine and Science in Sports and Exercise 23, 130–144.

Putnam, C.A., 1993. Sequential motions of body segments in striking and throwing skills—descriptions and explanations. Journal of Biomechanics 26, 125–135.

Sakurai, S., Ikegami, Y., Okamoto, A., Yabe, K., Toyoshima, S., 1993. A 3-dimensional cinematographic analysis of upper limb movement during fastball and curveball baseball pitches. Journal of Applied Biomechanics 9, 47–65.

Winter, D.A., 1990. Biomechanics and Motor Control of Human Movement, second ed. Wiley-Interscience, New York.

Yamane, K., Nakamura, Y., 2003a. Dynamics filter-concept and implementation of online motion generator for human figures. IEEE Transactions on Robotics and Automation 19, 421–432.

Yamane, K., Nakamura, Y., 2003b. Natural motion animation through constraining and deconstraining at will. IEEE Transactions on Visualization and Computer Graphics 9, 352–360.

Zajac, F.E., Gordon, M.E., 1989. Determining muscles force and action in multi-articular movement. Exercise and Sport Sciences Reviews 17, 187–230.

Zajac, F.E., Neptune, R.R., Kautz, S.A., 2002. Biomechanics and muscle coordination of human walking—Part I: introduction to concepts, power transfer, dynamics and simulations. Gait and Posture 16, 215–232.